MOLECULES ON CLEAN AND MODIFIED OXIDE SURFACES

H.-J. FREUND, T. KLÜNER, R. WICHTENDAHL, S. THIEL, M. ADELT,
W. DRACHSEL, M. BÄUMER, H. KUHLENBECK, T. RISSE, K. AL-SHAMERY,
M. KAMPLING, H. HAMANN
Fritz-Haber-Institut der Max-Planck-Gesellschaft
Faradayweg 4-6
D-14195 Berlin
Germany

Abstract

This paper reviews results obtained with a series of surface science methods on molecules adsorbed on well-ordered oxide surfaces. The experimental data are compared with calculations and it must be concluded that the understanding is far from satisfactory on a quantitative scale, although qualitatively some progress has been made. This is particularily demonstrated for photonstimulated adsorption of NO from NiO. In a second part oxide supported metal aggregates are studied with respect to morphology, geometric, electronic and magnetic structures. Their interaction with adsorbed molecules is a further topic. Size dependent properties such as CO dissociation probability and photonstimulated methan dissociation are discussed.

1. INTRODUCTION

In recent years many groups [1-7] have studied the properties of well-ordered oxide surfaces. Even though some qualitative understanding has been gained we are still far from a quantitative description even for the socalled simple systems.

We use the interaction of diatomic molecules with (100) surfaces of a rocksalt oxide (e.g. MgO, NiO) as an example to demonstrate the degree of convergence between experimental data and theoretical calculations on ground state properties such as adsorption energies [8]. For the specific system NO/NiO(100) we then go on to demonstrate that also excited state properties may be described [9-10]. In particular the results of photonstimulated desorption experiments including state specific detection of the desorbing molecules are discussed on the basis of *ab initio* calculations making use of wave-packet dynamics.

N. Russo and D.R. Salahub (eds.), Metal-Ligand Interactions in Chemistry, Physics and Biology, 91–128.

Clean oxide surfaces may be modified by deposition of metal aggregates [3-7]. By such a procedure model systems for catalytically active materials may be taylored. A wide variety of results referring to a morphological as well as a structural characterization of the system are applied. We analyse electronic and magnetic properties but also the chemical activities of such systems. In particular we are dealing with size dependent properties, and two examples, one for a thermal chemical reaction, and a second for a light induced reaction are discussed.

2. MOLECULAR ADSORPTION AND DESORPTION

2.1. Molecular adsorption

Molecules bind to oxides via a bonding mechanism considerably different from metal surfaces. A CO molecule, for example, binds to metals via chemical bonds of varying strength involving charge exchanges [11]. Figure 1 illustrates the bonding of CO to a Ni-metal atom via the so-called σ -donation/π-backdonation mechanism on the basis of a one electron orbital diagram.

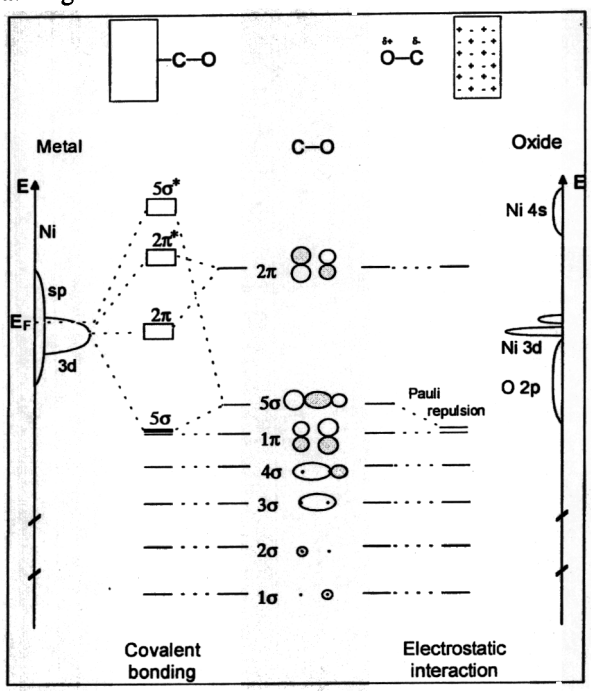

Figure 1. Orbital diagram for the bonding of CO to Ni-metal (left) and to Ni-oxide (right)

The σ- and π-interactions lead to a relative shift of those σ- and π-orbitals involved in the bond with respect to those orbitals not involved. The diagram reflects this via the

correlation lines. This may be contrasted by the electrostatically dominated interaction between a CO molecule and a Ni ion in nickel-oxide [12-13]. There is a noticeable σ-repulsion between the CO carbon lone pair and the oxide leading to a similar shift of the CO σ-orbitals as in the case of the metal atom, however, there is no or little π-backdonation so that the π-CO-orbital are not modified [6]. Conceptually, the situation is transparent and one would expect that a detailed calculation reveals the differences quantitatively . However, as it turns out the description by *ab-initio* calculations is very much involved and today a full account cannot be given [8]. This has to do with the fact that reliable experimental information is only available very recently. Theoretically the prediciton is that CO as well as NO bind very weakly to NiO [8]. The predicted binding energy is of the order of 0.1 eV and it is expected to be similar to CO binding to MgO(100) i.e. the influence of the Ni d-electrons is negligable [8]. Experimentally it is found that the influence is substantial. Table 1 collects the binding energies of CO and NO on MgO and NiO as determined from thermal desorption measurements on UHV-cleaved single crystal surfaces and thin films.

	MgO		NiO	
	Bulk	Film	Bulk	Film
CO	[14], 0.13 [15]	0.43 [16b]	0.31 [15]	0.32 [18] 0.43 [16a]
NO			0.57 [15]	0.52 [19]

Table 1: Binding energies (in eV)

Clearly, there is a difference between MgO and NiO with binding energies on NiO being systematically and significantly larger. This also correlates with shifts in the infrared frequencies of the corresponding stretching modes [20]. There is an indication that for NO more so than for CO there is a contribution of the π-system to the bond leading to chemical shifts to lower frequencies [21]. Pure electrostatic interaction would lead to shifts to frequencies higher than the gas phase [22]. Also, for the NiO system the binding energy values determined for the UHV-cleaved single crystal surface correlate very nicely with those data gained for carefully prepared thin films [15, 18, 19]. This is not always the case as is revealed for the MgO system [15, 16]. It is not fully clear at present what the reason for this discrepancy is but very likely, the films contain a considerable amount of defects. More work to disentangle the effects of defects on adsorption and a quantitative determination of binding energies on defect sites has to be performed. Thin films have been used to apply quantitative methods for structure determinations of adsorbates. Lindsay et al. [23] have recently reported photoelectron diffraction measurements for NO on a thin NiO(100)/Ni(100) film. They found a tilted NO molecule, N-end down located atop a Ni ion. The Ni-N bond distance is 2.81 Å and the bond tilted by about 50° with respect to the surface normal. This result is fully compatible with our early more qualitative studies on this system dating back to 1991 [19]. Theory had predicted this tilted NO bonding geometry including a chemical component to the molecule surface bonding [19, 21]. However, again in this case the calculated binding energies are by far too small. The NO/NiO calculations indicate that electron correlation plays a major role in the description of the bonding and it may well be that such

phenomena are the cause for the difficulties in a proper theoretical description of molecule-oxide bonding. In a chapter further below we will describe in detail how this surface molecule bond can be broken via photon stimulated processes, and how the particular bonding characteristics influence the dynamics of the bond breaking process.

It is, of course, interesting to move from simple diatomic adsorbates to more complex systems. We have investigated in great detail the interaction of a variety of molecules with the $Cr_2O_3(0001)$ surface [24, 25]. This surface was prepared on top of a thin $Cr_2O_3(0001)/Cr(110)$ film [26, 27]. We would only like to mention a study on adsorption of ethylene in connection with low pressure polymerization, where we have taken the chromia surface to model the Phillips catalyst – well knowing that it is a much more complex system [28]. We will briefly discuss some results gained for CO_2 adsorption because they reveal some interesting electronic properties of that particular surface [25].

CO_2 adsorbs on Cr_2O_3 non-dissociatively forming a moderately weak chemisorption bond which can be broken by heating the surface to slightly above room temperature, i.e. indicative of a binding energy near 1 eV. There is another state of adsorption with much lower binding energy closer to the value found for CO on NiO [18].

Figure 2 shows infrared spectra of CO_2 on $Cr_2O_3(0001)$ [25]. The more strongly bound species gives size to the band at 1200 cm^{-1} while the more weakly bound species leads to sharp band at 2300 cm^{-1}. While the latter is typical for an geometrically weakly or undistorted linear CO_2 molecules, the former bands are indicative of carbonates and/or carboxylates. Isotopically labelled CO_2 lead to shifts compatible with molecular adsorption. Oxygen preadsorption is known to block the metal sites at the surface leading to the formation of chromyl groups. They lead to the sharp peak near 1000 cm^{-1}. Interestingly, after oxygen preadsorption the chemisorbed CO_2 species does not form at moderate exposures. Obviously, CO_2 binds to the metal ions and not to oxygen. This is corroborated by absorbing $^{12}C^{16}O_2$ onto a Cr_2O_3 film made from isotopically labelled $^{18}O_2$. If a carbonate were formed we would expect an isotopic shift due to the involvement of the lattice oxygen in carbonate formation. This is not observed and we conclude that a carboxylate and not a carbonate is formed. This is somewhat surprising in view of the fact that the formation of a carboxylate involves partial or full transfer of an electron from a metal cation. However, we have found before that the chromium ions in the surface accumulate charge closer to Cr^{2+} and not to Cr^{3+} as in the bulk [26]. The low oxydation state mainly comes about through chromium-oxygen hybridization. Therefore it is not unlikely that the chromium ions in the low oxidation state partially transfer electrons to support the formation of a chemisorbed carboxylate.

The reason why the chromium ions in the surface assume a lower oxidation state has, very probably to do with the fact that the $Cr_2O_3(0001)$ surface is a depolarized polar surface which undergoes massive surface relaxations. A full structure determination via a LEED analysis of the surface has been performed [29].

An experimental hint towards the peculiar electronic structure of the surface is revealed by electronic EELS spectra (not shown here) [30, 31]. A surface state is observed in the optical band gap which is broad and has high intensity so that it is most likely not due to a Cr d-d-transition but rather due to surface charge transfer state connected with chromium–oxygen by oxidation.

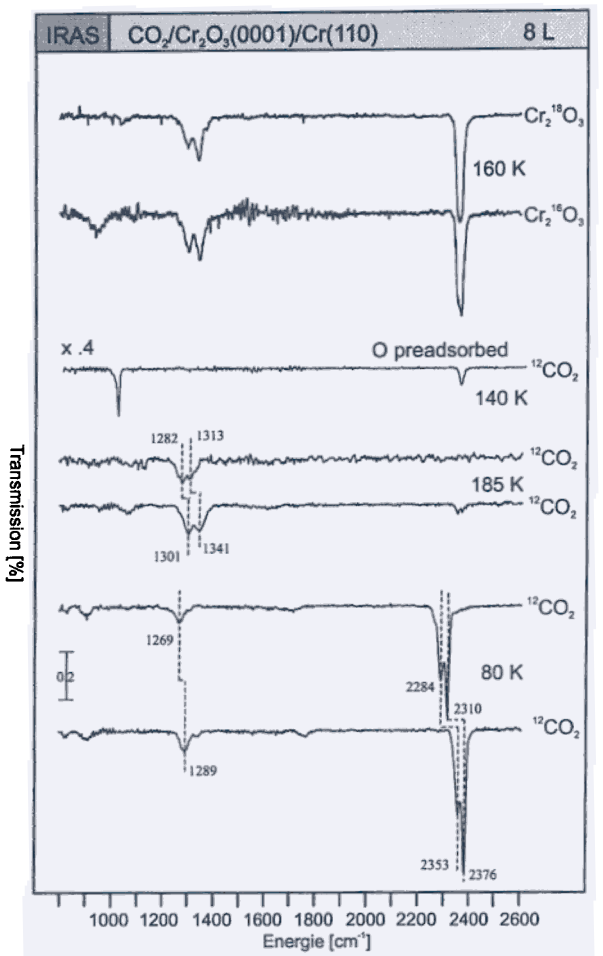

Figure 2. Infrared Spectra of CO_2 on $Cr_2O_3(0001)$

2.2. Molecular Desorption

Numerous experimental studies on quantum state resolved laser induced desorption of small molecules from well-characterised surfaces have been reported within the last few years [32] and a great amount of data has been obtained for these DIET (Desorption Induced by Electronic Transitions) phenomena. In most of these studies, various metals and semiconductors have been chosen as a substrate and usually small molecules like CO and NO were desorbed after laser irradiation. The major part of our experimental studies dealt with DIET phenomena on transition-metal oxide surfaces i.a. the system discussed above. We have investigated velocity distributions for different vibrational (v´) and

rotational (J´) states of the desorbing NO molecules (Figure 3) [33]. Some of the experimental result have already been summarised in a previous article within this series [34].

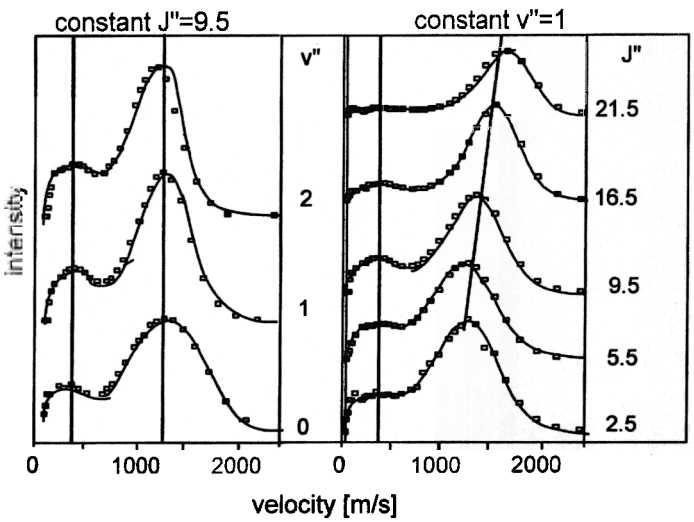

Figure 3. Experimental quantum state resolved velocity distributions of NO molecules after laser induced desorption of NO from NiO(100).

In the following paragraphs we want to focus on the theoretical description of quantum state resolved laser induced desorption of small molecules It turns out that even a qualitative understanding of the experimental results requires the development and application of state of the art theoretical chemistry, efficient algorithms and modern computer technology. Much progress has been achieved since the early days of DIET, when the famous MGR [35] model and its extensions [36-45] have been developed.

Recently, we reported *ab-initio* calculations for the system NO/NiO(100), in which a successful calculation of excited states involved in UV-laserinduced desorption has been performed [10]. In the remainder of this section we will focus on the theoretical description of these states, the characterisation of the corresponding potential surfaces and the consequences for the dynamics of the nuclear motion. It will be shown that a quantitative simulation of experimental final state distributions is possible on a first principles basis. Furthermore, a qualitatively new mechanistic insight into the desorption process can be obtained providing a physically intuitive picture on a microscopic level.

2.2.1. Methods of Calculation

In contrast to the calculation of the electronic ground state, density functional theory cannot be easily applied for the description of excited states in a straightforward manner. Therefore, ab initio cluster calculations using a NiO_5^{8-}-cluster embedded in a semi-infinte field of point charges ±2 are performed in order to describe the NiO(100)

surface (Figure 4). The point charges are chosen to be consistent with a Mulliken population analysis of the nickel and oxygen ions, respectively. The NO molecule is adsorbed at an on-top position above a Ni^{2+} cation. The $^2A'$ electronic ground state is characterised by an equilibrium geometry of 45° of the molecular axis with respect to the surface normal in perfect agreement with experimental data [19].

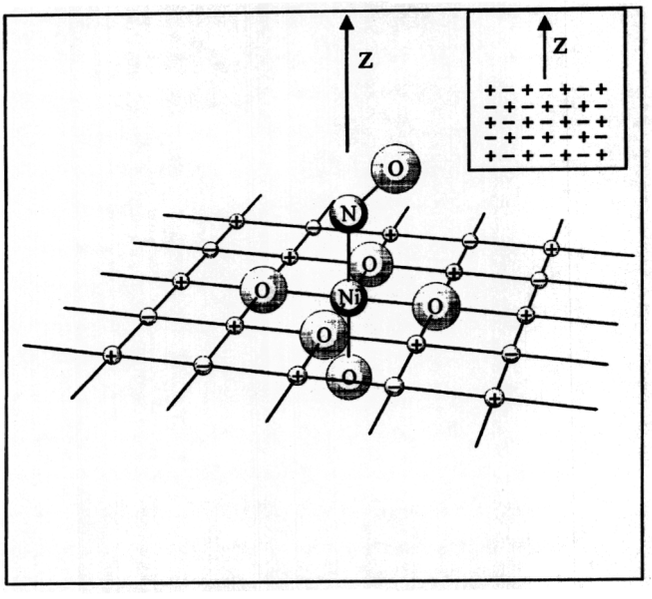

Figure 4. The NiO_5^{8-}-cluster embedded in a semi-infinite potential of point charges ±2 (only the topmost layer is shown).

The excited states relevant for the laser induced desorption of NO from NiO(100) turn out to be charge transfer states, in which one electron is transferred from the cluster to the adsorbed NO moleclue. This results in an NO^--like intermediate, which is described as a highly excited electronic state of the cluster/adsorbate complex. These excited states are obtained by performing configuration interaction (CI) calculations, in which the reference configuration consists of the valence space of the O2p-, Ni3d and NO2π-orbitals. The configuration space is generated from this reference determinant by single and double excitations. Technical details on the construction of the CI space and on the selection of a representative excited state are described elsewhere [10, 46].

By varying the distance R of the centre of mass of the molecule from the surface and the tilt angle α (polar angle) of the molecular axis with respect to the surface normal, a two dimensional PES for a representative NO^--like state is constructed. The PES is illustrated in Figure 5. The analytical form is given elsewhere [10, 47, 48].

The potential corrugation with respect to the azimuth angle β turns out to be small. Therefore, this coordinate is not considered in the construction of the PES. The internal N-O distance is kept fixed at the value of 2.175 a.u., which corresponds to the equilibrium

distance of the NO-molecule in the gas phase [49]. This is a reasonable first guess, since the internal NO vibration is decoupled from rotation and translation. This is obvious from the velocity distributions (see Figure 3), because the shape of the distributions does not depend on the vibrational state of the desorbing molecules. Therefore the vibrational excitation of NO after laser induced desorption can be investigated separately as described in paragraph 4. In contrast to this, the rotational coordinate α has to be taken explicitly into account, since there is an obvious correlation between translation and rotation (Figure 3), i.e. the faster the molecules desorb the higher is their rotational excitation.

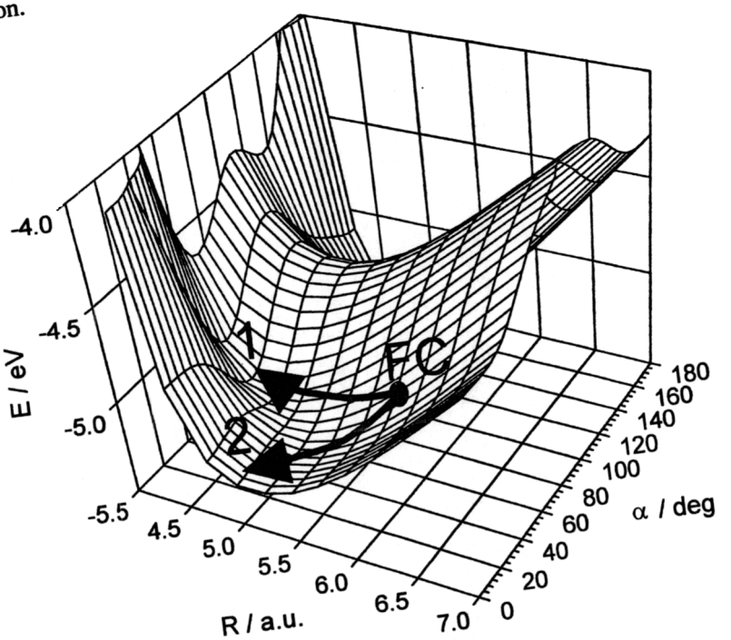

Figure 5. NiO(100)/NO: Charge transfer potential energy surface as a function of the distance R of the molecule from the surface and the polar angle α.

The ground state PES is constructed by adjusting the topology of the potential used in [50] to ab initio results. It is characterised by an equilibrium geometry of R=5.5 a.u. and α=45° with a binding energy of 0.52 eV. Details on the construction of the PES can be found in [47]. The excited state PES is calculated as described in the previous paragraph. Once the relevant potential energy surfaces have been obtained, the dynamics of nuclear motion is calculated by solving the time dependent Schrödinger equation for the nuclei. We performed three dimensional wave packet calculations, where the distance

R of the molecule from the surface, the tilt angle α (polar angle) and the corrugation angle β (azimuth angle) are included. In all calculations, the Chebychev polynomial expansion of the time evolution operator is used [51].

The rotational vibrational ground state wave function of the electronic ground state is taken as the initial wave packet for the propagation on the ab initio excited state PES (Franck Condon transition), for which the wave packet is a non eigenstate. The desorption scenario is simulated by transferring the wave packet after propagation for a residence lifetime τ_R on the excited state to the ground state PES (wave packet jumping). The desorbing part of the wave packet is finally analysed in the asymptotic region of the ground state PES, where state resolved velocity distributions are calculated. An incoherent stochastic average scheme for different residence lifetimes τ_R of N quantum trajectories is applied introducing the (spectroscopic) resonance lifetime τ as a parameter [52]. All calculated observables exhibit a parametric dependence on the resonance lifetime τ.

2.2.2. Desorption dynamics

The major goal of the present study is the understanding of the shape of the velocity distributions on a microscopic level. Especially the question of the origin of the bimodality of the distributions has to be addressed. Furthermore the coupling between translation and rotation of the desorbing molecules has to be explained.

Figure 5 shows the charge transfer potential surface, where the Franck Condon point (the starting point of the wave packet after the transfer to the excited state) is denoted by FC. The topology of the PES can be understood as a result of an interplay between Coulomb attraction between NO^- and the hole created in the surface upon electron transfer and the Pauli-Repulsion of the diffuse charge distribution of NO^- and the O^{2-} anions within the surface [53]. By inspecting carefully the topology of the PES, the experimental results can be explained in a physically appealing manner. Since the minimum of the charge transfer state is located at a smaller molecule-surface distance R than in the electronic ground state the molecule is accelerated towards the surface after electron transfer from the surface to the NO molecule resulting in an Antoniewicz-like desorption scenario [54]. Additionally, the Pauli-Repulsion results in a preference of a linear adsorption geometry at relevant molecule-surface distances. This is illustrated in Figure 6.

As indicated in Figure 5 two pathways exist for the time evolution of a wave packet on the charge transfer PES. A part of the wave packet follows way 1 probing the valley of the potential surface gaining a large amount of kinetic energy, whereas another part of the wave packet follows pathway 2 and is deaccelerated quite early due to the repulsive topology of the potential gaining a small amount of kinetic energy. This effect can indeed be observed when a wave packet is propagated for a certain lifetime and the velocity distribution is calculated for a particular quantum state as shown in Figure 7. In addition to this, partial wave packets taking pathway 1 find themselves in a more repulsive region

of the ground state potential after relaxation compared to partial wave packets taking way 2. Therefore, the bimodality in the final state velocity distributions can be traced back to a bifurcation of the nuclear wave packet due to the PES involved.

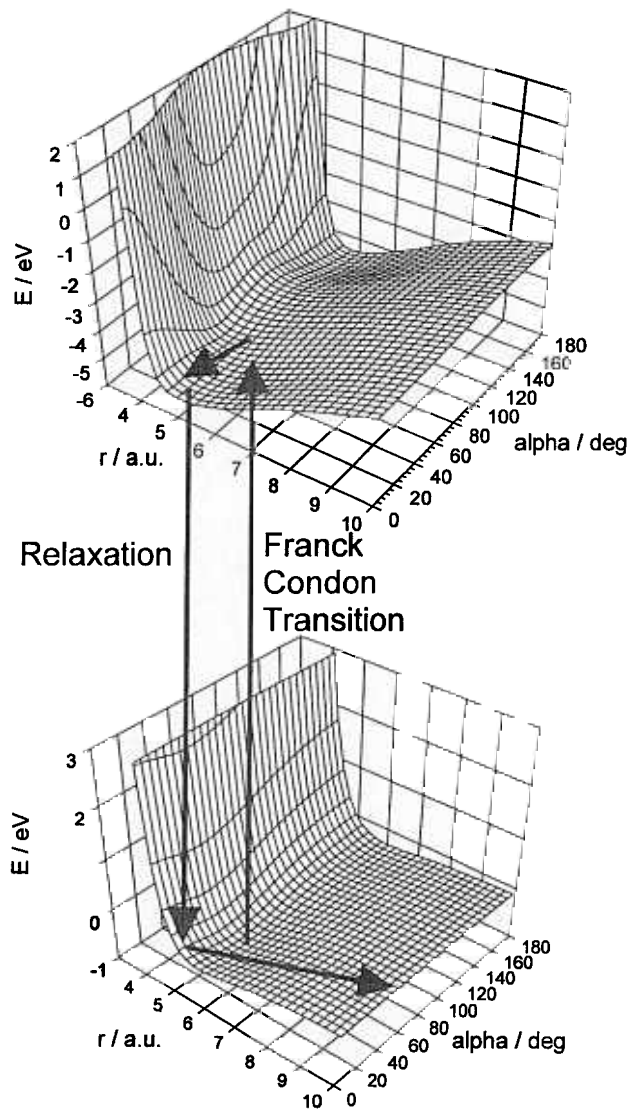

Figure 6. NiO(100)/NO: Desorption scenario of the Antoniewicz type with preference for a linear adsorption geometry in the excited state.

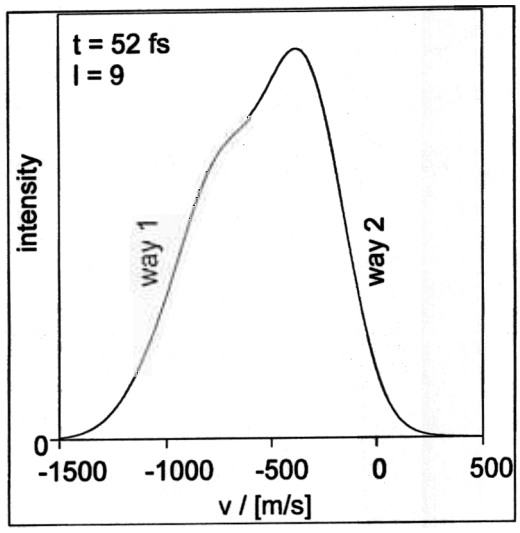

Figure 7. Velocity distribution for an angular momentum quantum number l = 9 after a residence lifetime of 52 fs on the excited state potential.

Up to now, we discussed the possible consequences of a wave packet propagation only qualitatively. To obtain quantitative results, the stochastic wave packet jumping procedure described above has to be applied and the only parameter τ (resonance lifetime) within this averaging scheme has to be chosen correctly. We assume the lifetime of the negative ion resonance to be about 25 fs, since the desorption probability, i.e. the square norm of the wave packet in the asymptotic ground state potential region, turns out to be P_{des} = 3.3%, which is in reasonable agreement with experimental results for oxide systems [10]. Using the same value for τ, we obtain the state resolved lifetime-averaged velocity distributions as shown in Figure 8. Compared to the experimental distributions in Figure 3 all relevant features can be simulated [10]. The distributions are clearly bimodal, are in the correct velocity range and even the coupling between translation and rotation in the fast desorption channel is reproduced.

As demonstrated above, wave packet studies on the basis of our ab initio potential surfaces allow a quantitative simulation of the experimental final state distributions by introducing the lifetime of the negative ion resonance as the only parameter. Furthermore a microscopic insight into the desorption scenario has been gained on a first principles basis.

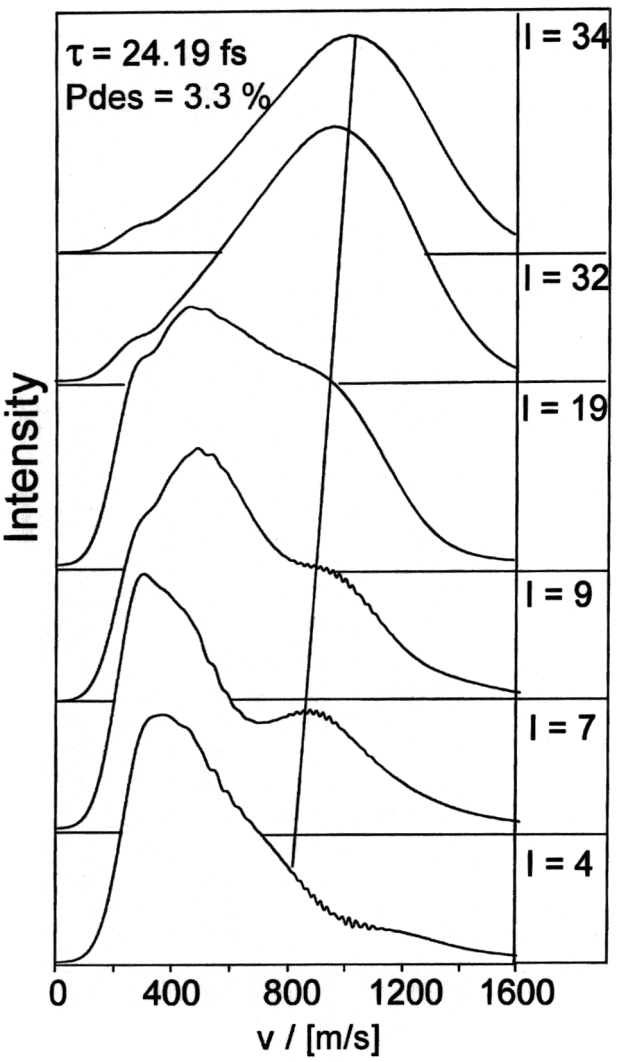

Figure 8. Velocity distributions for a resonance lifetime of 24.19 fs for different rotational quantum numbers l.

So far, the internal N-O coordinate has not been taken into account, because of the reasons mentioned in the previous paragraphs. In this section we want to clarify, weather our calculations, which predict an NO^- to be the intermediate species occurring in the desorption process, are consistent with the vibrational excitation of the desorbing NO-molecules.

Experimentally, a high vibrational excitation is observed (relative vibrational populations: $P_1/P_0 = 0.17$, $P_2/P_0 = 0.06$), corresponding to a temperature of T_{vib}=2000 K indicating a non-thermal excitation mechanism. The equilibrium bond length of the adsorbed NO-molecule has to be significantly different from that of the intermediate. However, it has been pointed out by Zimmermann [32], that simply assuming gas phase values for the equilibrium distances for NO (r = 2.175 a.u.) and NO^- (r = 2.377 a.u.) respectively [49], results in a vibrational excitation, which is much too high ($P_1/P_0 = 0.42$, $P_2/P_0 = 0.33$) compared to the experimental values [9, 33]. It was concluded that only a partial transfer of charge can take place and a transfer of a full electron seems unlikely. This is in contrast to our ab initio studies, since the analysis of CI-wavefunction yields a full charge transfer.

In order to solve this problem, we performed Hartree Fock calculations of NO and NO^- above different point charge fields representing the NiO crystal. The electrostatic fields are describing either a neutral surface (before charge transfer) or an ionised surface (after charge transfer). The generation of these field is described in reference [53]. The internal N-O distance was varied to find out, weather the equilibrium distance of NO or NO^- above the point charge fields is different from the gas phase values.

In case of the neutral NO-molecule, we observed only minor changes in the bond length due to the electrostatic field. On the other hand NO^- above the ionised surface exhibits a strong polarisation of the 1π-molecular orbital towards the nitrogen atom. In the gas phase, the 1π-orbital has a lone pair character, since most of the electron density is located at the oxygen atom. Due to the strong polarisation by the electrostatic field above the surface this orbital gets a bonding character and a charge equivalent of half an electron is transferred from oxygen to nitrogen [55]. This field induced bonding character of the 1π-orbital results in a bond length contraction of about 0.20 a.u. as indicated in Figure 9.

Taking this field effect into account, we calculated the relative vibrational populations to be $P_1/P_0 = 0.20$ and $P_2/P_0 = 0.06$ as described in reference [55]. In conclusion, a quantitative agreement between experimental and theoretical results is obtained within the model of a fully negatively charged intermediate for the NO/NiO(100) system, when electrostatic field effects are taken into account.

Summarizing, in this chapter we focused on the progress in the theoretical description of laser induced desorption. We showed for the first time that a consistent simulation of all relevant experimental observables (shape and range of velocity distributions, coupling of rotation and translation, desorption probability, vibrational excitation of desorbing molecules) is possible on a first principles basis. A new mechanistic insight has been gained in the desorption mechanism especially with respect to the origin of bimodal velocity distributions and the question, weather NO^- can be a possible intermediate during photoinduced desorption. It turns out that the ab initio description of excited charge transfer states is crucial even for a qualitative understanding of the desorption scenario, since the topology of the potential surfaces involved is most important but rather complicated and cannot be obtained (semi-) empirically.

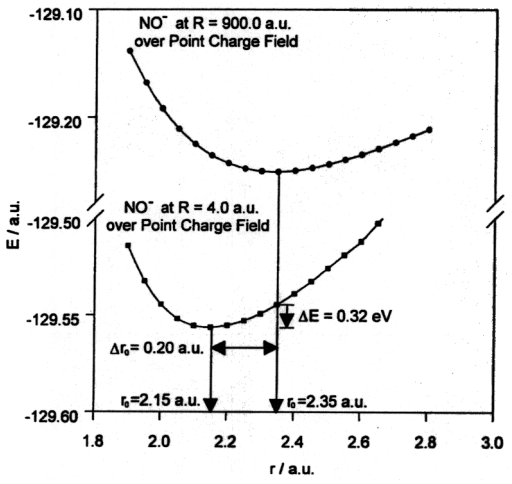

Figure 9. Hartree Fock potential curves as a function of the internal NO-distance r. R denotes the distance of NO^- from the field.

3. METALS ON OXIDE SURFACES

The growth of metals on oxide substrates has been the subject of many studies in the past (e.g. see the review article of Campbell [4] and references cited therein). One of the reasons for the interest in these systems results from the potential they have as model systems for supported metal catalysts, since they facilitate a detailed investigation of the interplay between the structure of such composite systems and their interaction with adsorbates.

There are several examples showing that it is within reach to establish correlations between particle size and electronic properties on the one hand and adsorption behavior or catalytic activity on the other hand [56, 6].

Typical metal support systems are those in which the metal is a transition metal, and the support is, for example, composed of SiO_2, Al_2O_3, or MgO. We can produce well-ordered layers of MgO [16a, 57-65] and Al_2O_3 [66-74]. The preparation of ordered SiO_2 layers still gives difficulties [75]. We have focused our attention until now on the support system Al_2O_3, and thus in the following, initially the structure and properties of the support [66, 71], as well as the possibilities of its chemical modification by functionalization [76] will be considered, and thereafter the growth, morphology, electronic and magnetic structure as well as adsorption, and reaction behavior of the metal films deposited [76-87].

A well-ordered, thin Al_2O_3 film can be generated on a (110) surface of a NiAl alloy single-crystal by oxidation and tempering at 900 K [66, 71]. The stoichiometry of the film corresponds within the limits of experimental error to that of Al_2O_3 [66]. Photoelectron spectroscopy and EEL spectroscopy were used to show that the film contained no metallic Ni and no NiO [66]. The film is chemically unreactive, and CO adsorbs on it only at low

temperatures (< 80 K) [68, 69], whereas CO binds to the NiAl substrate up to significantly higher temperatures [88, 89]. Thermal desorption studies confirm that the film formed covers the whole surface of the alloy.

The film is oxygen terminated and tetrahedrally and octahedrally surrounded Al ions are present.

The film prepared in this way can now be directly covered with metal, but it can also be chemically modified prior to the introduction of the metal [76]. Thus, it has been possible to study the influence of functional groups on the Al_2O_3 surface on the growth and reactivity of thin metal films. Of special significance in this context are hydroxyl groups on the Al_2O_3 surfaces [72, 76, 90-97].

4. MORPHOLOGY OF METAL DEPOSITS

Figure 10 shows several examples resulting from metal deposition on a thin alumina film.

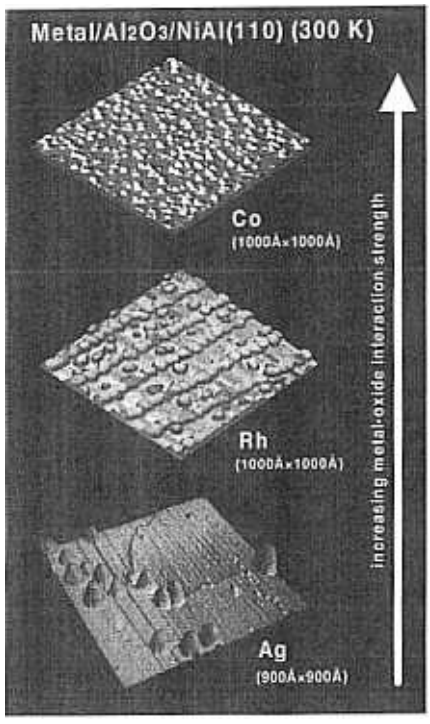

Figure 10. STM images of Co, Rh and Ag deposited on Al_2O_3/NiAl(110) at 300 K.

Remember that for the function of catalysts the morphology and structure of the metal deposits is very important because it determines the activity and selectivity in the chemical process. Different metals exhibit very different growth modes which depend to a large extent on the strength of interaction between the metal and the oxide substrate. This in turn is strongly influenced by the presence of defects, such as steps or domain boundaries or point defects on the substrate. Silver as an example only weakly interacts with alumina and is consequently very mobile at room temperature. It nucleates at steps and forms relatively large but only few aggregates (bottom of Fig. 10). Platinum or cobalt and nickel, on the other hand, while interact more strongly with the oxide substrate, are less mobile and thus form small particles upon deposition at room temperature (top of Fig. 10). Such investigations give direct indications how the substrate has to be conditioned for a given metal in order to prepare a certain dispersion of metal particles. The adsorption energy E_{ads} is described by the classical Young approximation [96-98], for which approximate values are known for the first two interaction energies, but the oxide/metal term is usually not known.

$$E_{ads} = E_{oxide/gas} + E_{metal/gas} - E_{oxide/metal} \qquad (a)$$

Whether the metal particles are mobile at a given temperature depends on E_{ads}. If $E_{ads} < 0$, full coverage is attained, that means a layer growth of the Frank-van der Merwe type. If $E_{ads} > 0$, three-dimensional islands are formed (Volmer-Weber growth mode) [98]. If a layer-by-layer growth is replaced at a known layer thickness by a three-dimensional growth, it is referred to as a Stranski-Krastanov mode. Naturally, the detailed defect structure of the substrate and the introduced particles play an important role for these processes, since the defects of the oxide layer are nucleation centers for the deposited particles, as is apparent from Fig. 10 (middle panel).

However, it is not just a question of the existence of defects per se but also their nature. Palladium, for example, has a growth behavior that is influenced by the existence of domain interfaces, as well as by the steps in the substrate and point defects in the oxide layer [83]. This is illustrated in Fig. 11a, in which Pd was deposited at 90 K.
The Pd particles partly decorate the domain interfaces, as can be seen in the figures. In addition, there are particles on the terraces. If the same amount of Pd is separated off at room temperature, the mobility is increased and clearly larger aggregates form. Some of the aggregates in Fig. 11b adopt the shape of small crystals. That these crystals are limited by planes with a (111) orientation is apparent from the electron scattering diagrams, such as that shown in Fig. 11c [83]. The oxide reflections are two diffuse, but clearly definable, hexagonal (111) superstructure reflections rotated 12° towards each other. The double reflections stem from the growth of the particles on both the Al_2O_3 domains. Recently, we have studied some aspects of the internal structure of the aggregates. Using transmission electron microscopy, it has been found that the average lattice constant of the aggregates decreases as a function of decreasing aggregate size. The magnitude of the effect depends on the particular metal and varies between 3 - 8% with respect to the bulk lattice constant [99-101]. Also, it has been possible to atomically resolve terraces of some aggregates but

imaging the entire island including the atoms at the oxide metal interface is still difficult [102].

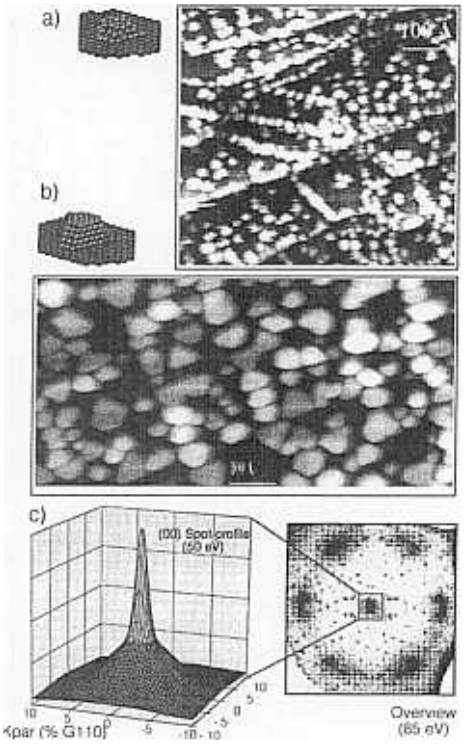

Figure 11. Pd growth on Al_2O_3/NiAl(110) : a) STM image after Pd deposition at 90 K (CCT, +1.6 V, 2.2 nA). b) STM image after Pd deposition at 300 K (CCT, +0.4 V, 0.5 nA). c) LEED pattern after deposition of 20 Å Pd at 300 K (right hand side) and intensity profile of an area close to (00)-spot (left hand side).

Rhodium which is an important component in car exhaust catalysts exhibits a slightly stronger interaction with the substrate as compared with Pd. In the middle panel on the left of Fig. 10 rhodium has been deposited at room temperature on the clean alumina substrate. The mobility of rhodium at this temperature is such that the aggregates nucleate at the defects without coalescence due to the particular epitaxial growth conditions forming strings of deposited aggregates. In order to grow aggregates in a random distribution across the surface one could expose the surface at lower temperature as shown in Fig. 12 or hydroxylate the surface before exposure to the metal vapor [103]. If the latter is done, the impinging rhodium atoms chemically bind to the hydroxyl groups according to the reaction scheme

$$\{Al^{3+}\,OH^{-}\} + Rh^{0} \rightarrow \{Al^{3+}\,O^{2-}\}\,Rh^{+} + H_{ads} \qquad \text{(b)}$$

and this stabilizes smaller aggregate sizes at random distribution even at room temperature, as shown in Fig. 13. Once the aggregates have been formed and have reached a given size, they are stable over a considerable region of temperatures.

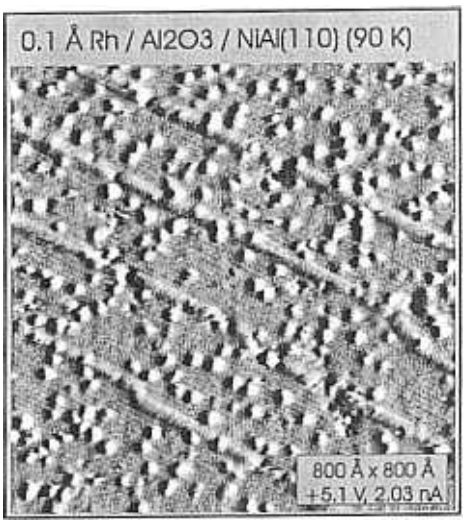

Figure 12. STM image of 1/20 monolayer of rhodium deposited at 90 K onto an alumina model substrate. The light protrusions represent the deposited metal aggregates. The structure of the oxidic support is represented by the finer structure and the broad linear features are due to antiphase domain defect structure at the surface.

For example, the distribution of aggregates created by deposition at low temperatures (70 K), shown in Fig. 12, is morphologically stable up to 700 K. The rhodium aggregates prepared on the hydroxylated surface (Fig. 13) are even more stable. We may use the region of thermal stability of the aggregates to investigate chemical reactivities of such an ensemble of aggregates without changing morphologies. This brings us in a position to study a particular chemical reaction for a given particle size under very well defined conditions and proceed a step towards bridging the above mentioned materials gap [6]. Furthermore, if we are able to control the size of the deposited aggregates, then we should be in a position to explore the size dependence of chemical reactions in such systems. In catalytic reactions particle size selectivity of reactions has been used to steer these reactions to certain products. CO dissociation has to be considered one reaction channel in connection with automotive exhaust control because it can lead to the deposition of carbon on the catalyst which in turn may poison its activity. We have chosen to investigate this very simple reaction, i.e. CO dissociation on rhodium aggregates. It is known from the study of the interaction of CO with rhodium aggregates deposited on alumina powders that CO shows a varying tendency to dissociate into carbon and oxygen atoms apparently depending on the size of the deposited rhodium aggregates. By varying particle sizes via the methods of nucleation and growth of metal particles on the alumina

model substrate, we are now in a position to study the particle size dependence of this simple reaction in detail. The result of such a study is shown in Fig. 14.

Figure 13. STM image of 1/2 monolayer of rhodium deposited at room temperature onto a prehydroxylated alumina model substrate. In comparison with the rhodium deposit in Fig. 10 (which represents the non-hydroxylated surface) the distribution is more uniform

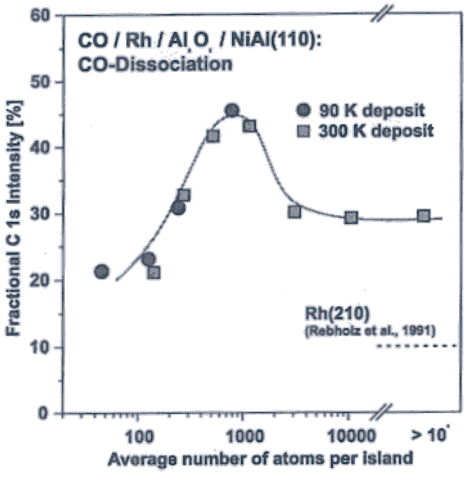

Figure 14. Plot of the C1s intensity resulting from the dissociation of CO (adsorbed at 90 K, heated to 600 K) as a function of the average number of atoms per particle.

The main result is the maximum in the dissociation rate observed for aggregates containing about 1000 atoms while for smaller as well as larger aggregates the dissociation rate is lower. It is well known for flat metal single crystal surfaces that CO does not dissociate upon adsorption but rather binds to the surface reversibly as a molecule. The introduction of steps on the surface is known to induce dissociation indicating that there are specific sites necessary for the dissociation reaction. A detailed analysis of the structure and morphology of the deposited aggregates as a function of size indicates that it is the creation and finally the diminution of steps that steers the reactivity. Again, resorting to Fig. 14 and following the dissociation rate curve from the left it has been shown that the smallest particles grow as two-dimensional layers and before the aggregates contain 100 atoms, the second layer starts to grow. Eventually, three dimensional particles grow but their height never exceeds their width. When the particles contain less than about 1000 atoms, the particles coalesce and the island density decreases considerably. This is when the dissociation rate decreases and the maximum has been surpassed. Thus, it is quite easy to understand how the size-dependent reactivity comes about in this case. It turns out that the size of particles near 5 nm where we find highest dissociation rates indeed coincides with those sizes where high catalytic activities have been observed in various, also much more complex chemical reactions. Obviously, for a given metal/substrate combination certain particle sizes stabilize a maximum of active sites and thus maximizes the reaction rate. This, however, is only one ingredient in optimizing a catalytic reaction. Selectivity is another issue that has to be addressed in the future.

5. ELECTRONIC STRUCTURE AND ADSORPTION

Photoelectron spectra can be taken of the systems morphologically characterized in this way [84-87]. As well as with valence ionization also in the area of ionization of inner shell electrons the dependency on the particle size can be established. We discuss for the clean adsorbate free particles only the inner ionization. Figure 15 summarizes for Pd deposits some 3d spectra, which were taken with synchrotron radiation.

The binding energy and the line width observed for the largest aggregates are practically the same as that of the solid Pd(111) surface. One observes a clear shift to higher binding energies with decreasing particle size and at the same time a clear line broadening. Many effects could contribute to both of these observations [105-107]. Generally it can be said that charge transfer phenomena as well as so called initial state effects and also such influences which come about in the ionized state of the system could play a part. The discussion of line widths turns out to be especially difficult [105, 106, 108-111]. One can at the moment only suspect that the non equivalence of the different metal atoms within the differently sized aggregates and the interaction of a part of the metal atoms with the substrate combined with the final state effects are responsible for the spread.

In contrast, the interpretation of binding energy shifts which are graphically summarized on the right of Fig. 15a for Pd aggregates and in Fig. 15b for Rh aggregates turns out to be in contrast somewhat clearer [107, 112]. Specific metal/support

interactions [110], in the sense, that charge is transferred from the metal to the support can be discussed using initial state effects.

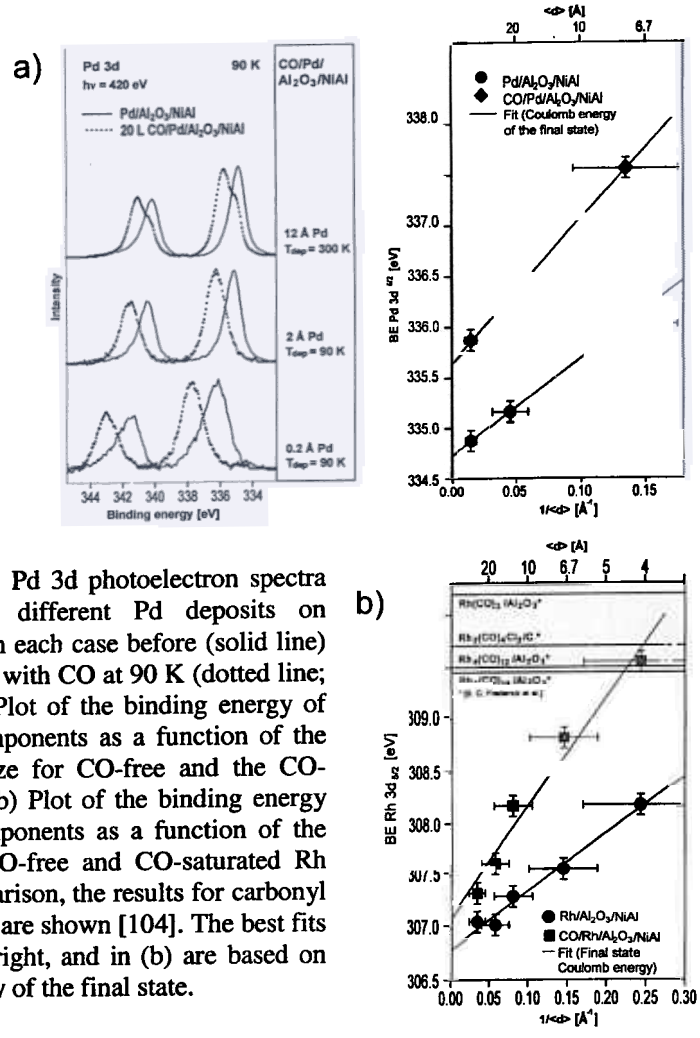

Figure 15. a) Left: Pd 3d photoelectron spectra (hν=420 eV) for different Pd deposits on Al_2O_3/NiAl(110), in each case before (solid line) and after saturation with CO at 90 K (dotted line; 20 L CO). Right: Plot of the binding energy of the Pd surface components as a function of the average particle size for CO-free and the CO-saturated systems. b) Plot of the binding energy of the surface components as a function of the particle size for CO-free and CO-saturated Rh deposits. For comparison, the results for carbonyl compound deposits are shown [104]. The best fits of the data in (a), right, and in (b) are based on the Coulomb energy of the final state.

radius of the particle [107, 112]

$$E_c \propto R^{-1} \qquad (c)$$

and the binding energy shifts to higher binding energies with smaller radii. There is a number of experimental results [105-112] which are in accordance with equation (c) along with the explanation of the binding energy shift described in Fig. 15b. The shifts are put down fundamentally to final state effects. One would expect with a pronounced influence of charge transfer processes in a non ionized system a strong influence on the bonding energy of the substrate, which lies however in our case at 10% of the total effect. Possible reasons why pronounced charge transfer effects were observed with Pd [113-115] and Ni deposits on Al_2O_3 layers which are on Al substrates, could be found for the different interactions on the metal/oxide interface with dependency on the defect density and stoichiometry of the film.

Binding energy shifts and line shapes change considerably if one adsorbs onto the metal deposits carbon monoxide. CO adsorption offers itself for study, because one has at one's disposal extensive comparative material of CO adsorption on metal single crystals [116-119]. Figure 15 compares the Pd 3d spectra with and without CO coverage for desposits at 90 K and 300 K. If one looks at the available spectra after CO saturated coverage at 90 K, the highest Pd coverage (corresponds to a mean island size of 70 Å) shows again clear parallels to the Pd(111) surface [120-122]. The Pd 3d signal of the clean surface shows a bulk and a surface component which are shifted towards one another by about 0.3 eV [116] and could not be resolved. CO adsorption leads to a shift of the surface component from ca. 1.1 eV to a higher binding energy whereby both sections (see shoulder in spectrum) could be well separated. The bulk portion amounts to 40% in this case, decreases to 13% with 2 Å Pd (average island size of 22 Å) and can no longer be distinguished with 0.2 Å Pd (average island size 7.5 Å). The comparison of the CO induced binding energy shifts shows that this grows with decreasing island size to ca. 1.5 eV. Experiments on single crystals show that the observed binding energy shifts depend on the number of coordinated CO molecules [120, 122]. Also a further analysis of the data [76] leads us to suspect that for smaller aggregates the number of coordinated CO molecules per surface Pd atom increases from one to two. The observed coordination numbers for transition metal carbonyls were never achieved [76]. Nevertheless where one is able to compare the metal ionization in carbonyl compounds with those from the deposited particles [104], the observed ionization energies from the carbonyl compounds with those of the smallest aggregate are in agreement. Figure 15b shows the comparison for Rh ionization. The obtained binding energies for the smallest aggregates are in agreement with the exact island sizes in the region of two to six nuclear metal carbonyls [104]. The well known $Rh(CO)_2$ species on an Al_2O_3 surface shows with 310.2 eV an even higher binding energy [104]. Owing to the limited comparability of the substrate used, barriers are naturally set to such a comparison.

Further indications to the electronic structure of the systems can be derived from the valence as well as the C1s ionization of the adsorbed CO and also from thermal desorption spectroscopy (TDS) but will not be discussed here.

The unique electronic properties of the deposited aggregates will however be discussed and are obvious from measurements where the aggregates are excited by electrons and the emitted light is spectroscopically collected [123]. The results of such cathode luminescence measurements are exemplified in Fig. 16 where a photograph of the experimental observation is shown together with two spectra recorded for two different average size distributions of deposited Pd aggregates.

The experimental set up is simple: The electrons are emitted from a cold field emitter tip and are accelerated towards the sample. The emitted light is collected via a spectrometer involving a l-N_2 cooled CCD camera. The light spot is the light emitted from the sample as observed by the naked eye. The spectra are complex and we refer to the literature for details [123]. Briefly, they contain a section up to 2.6 eV luminescence energy that involves excitations in the oxide/alloy substrate and another part between 2.6 and 5 eV which corresponds to emission from the deposited particles. The observed emission maxima change in energy position and intensity as a function of average aggregate size. This documents the quantum confinement of the electrons within the deposited metal aggregate as expected from a simple electron-in-a-box-approach. Detailed theoretical calculations have yet to be performed to allow for a final interpretation. One aspect is interesting with respect to a use of the light emitting properties of the aggregates, namely the expectation that these emissions could also be stimulated optically. This would allow us to probe the dynamics of electronic processes such as energy dissipation within the aggregate as a reaction is proceeding on the particle. We feel that the use of ultrafast lasers will help in the not too distant future to tackle some of these questions.

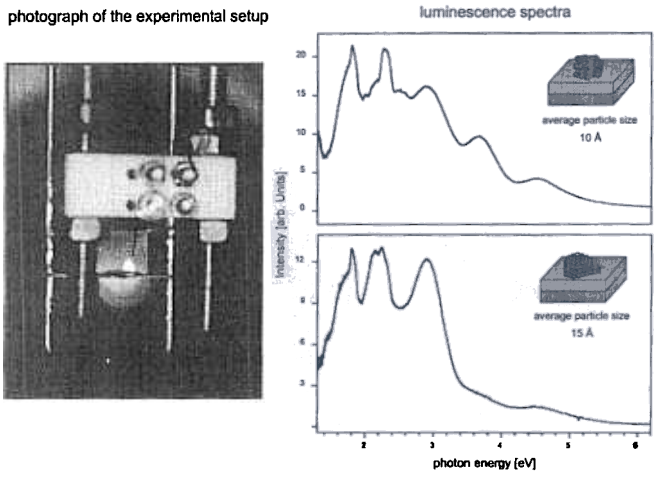

Figure 16: The photograph shows the rectangular probe with a luminescent spot on its lower part. The ceramic holder of the field-emitter tip as well as the emitter wire can be seen. Two cathodoluminescence spectra are shown for clusters with an average size of 10 and 15 Å, respectively. The high energy bands are characteristic for such small particles while the bands at lower energy are also found for the pure substrate.

6. ADSORBATE VIBRATIONS

Vibrational spectroscopy is considered to be one of the most powerful tools to investigate the interaction of small metal aggregates with molecules adsorbed from the gas phase. We only discuss here IR-studies for CO saturation on Pd aggregates [124]. Figure 17 contains corresponding data where on the left-hand side the Pd aggregates were grown at a substrate temperature near 90 K and on the right-hand side at a substrate temperature near 300 K.

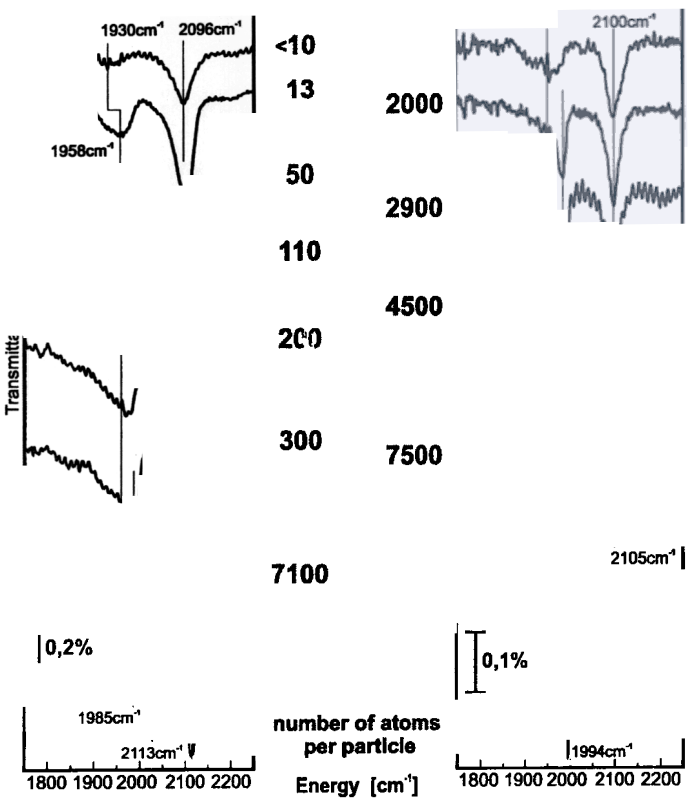

Figure 17. Series of IR-spectra taken after deposition of different amounts of Pd at 90 K (left) and 300 K (right) and dosage of 20 L CO at 90 K. The average number of atoms per particle is given next to the spectra.

The aggregates deposited at 300 K are crystalline with (111) facets parallel to the substrate. Such a situation can be described by aggregates of cubooctahedral symmetry [56, 83].

We note from Fig. 18 that the amount of adsorbed CO as judged by the integrated CO signal intensity is considerably larger for the low temperature Pd deposits than for the room temperature deposits for a given amount of deposited metal. This is due to the larger surface area exposed by the irregularly shaped aggregates deposited at low temperature. As a general observation from Fig. 17 we realize that the positions of the bands for deposits at both temperatures are comparable. Furthermore, the line widths observed in Fig. 17 are, perhaps not unexpectedly, larger for the low temperature deposits due to the inherent higher degree of microscopic heterogeneity of Pd positions in those aggregates. It is possible to assign three regimes of frequencies for both sets of deposits based on the spectra for saturation coverage shown in Fig. 17. Those regimes are: 1930-1970 cm^{-1}, 1970-2000 cm^{-1} and 2090-2120 cm^{-1}. On the basis of arguments presented below for the coverage dependent studies we assign these bands to bridge bonded species on the terraces of the aggregates (1930-1970 cm^{-1}), to bridge bonded species on the edges of the aggregates (1970-2000 cm^{-1}), and to terminally bonded CO (2090-2120 cm^{-1}) not necessarily situated on the terraces, of course. The bands that we assign to CO bridge bonded on the edges of the aggregates have previously been assigned to CO on Pd(100) sites [125-130]. The intensity of the absorption band in this region together with the results from earlier SPA-LEED and STM-studies [6, 83] lead us to a different interpretation (see below).

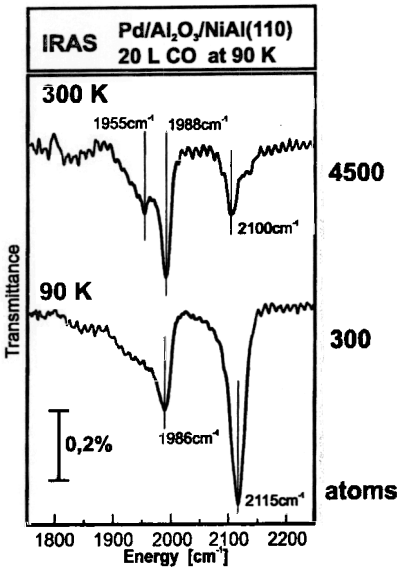

Figure 18. Spectra for 4.4 Å Pd (average thickness) deposited at 300 and 90 K and a dosage of 20 L CO at 90 K.

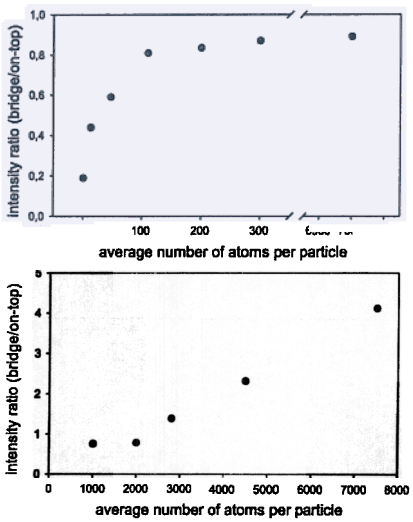

Figure 19. Ratio of the integrated intensities of the absorption bands for bridge and on-top bonded CO for the 90 K (top) and the 300 K (bottom) deposits as a function of particle size.

For the low temperature deposits there is a clear trend if we compare the intensity in the region of bridge bonded species with the intensity in the region of terminally bonded species as a function of aggregate size (Fig. 19, top). It is found that the fraction of bridge bonded species increases rapidly with the size of the aggregates until it reaches a saturation value. This is consistent with an increase of sites with two Pd atoms at the proper distance to be bridge bonded by CO molecules. If we compare this with the situation for the room temperature deposits also plotted in Fig. 19 (bottom), we realize the much slower increase starting from a higher level. Clearly, this is caused by the higher degree of order for the room temperature deposit already at the lowest metal coverage where the particles expose small terraces with atomic arrangements allowing for a considerable number of bridge bonds to be formed. Once the aggregates have assumed their regular shape, the relative ratio of bridge bonds to terminal bonds is only expected to change slowly [56, 83]. On the other hand, Pd(111) terraces bind CO molecules in a terminal geometry only at very high CO coverages ($\Theta > 0.7$) [71]. On Pd(111) the terminally bonded CO with an adsorption band at about 2100 cm^{-1} is always accompanied by an intense band at about 1900 cm^{-1} which is assigned to a species adsorbed on threefold-hollow sites [129, 130]. (The shift of this band from about 1830 cm^{-1} at very low CO coverages is caused by dipole coupling [131].) At this high coverage the population of bridge sites is extremely low on Pd(111) (see above). The peak at about 1900 cm^{-1}, characteristic for CO molecules bound in threefold-hollow sites at high coverages, is not found in our spectra with corresponding large intensity but, if at all, as a weak shoulder. On Pd(111) for coverages of about $\Theta = 0.6$-0.7 the amount of terminally bonded CO is nearly zero and the CO is predominantly bridge bonded (see above) [122].

Combining all arguments the spectra indicate on one hand that on the facets of the Pd clusters the saturation coverage is smaller than saturation coverage (Θ = 0.75) on a Pd(111) single crystal, and the CO molecules are preferentially bridge bonded on the aggregates. On the other hand, the above reasoning also explains why the intensity in the region of terminally bonded CO is considerably lower for the room temperature deposits, which exhibit well-ordered facets, i.e. because the coverage is below Θ = 0.75. In the spectral region assigned to the bridge bonded species there is a marked redistribution of intensity between the two sites, i.e. on the terraces and on the edges, favoring the edge bonded species for larger aggregates. This increase in intensity is too large to be understood on the basis of an increase in the number of sites [132] if we consider a cubooctahedron. We suggest here that it is due to dynamic intensity transfer via dipole coupling between the terrace bridge species with stretching frequencies at lower frequency towards the edge bridging species at higher frequency. Such an intensity transfer through dipole coupling would be consistent with what is known from single crystal [133-135]. It is also consistent with the trend observed in Fig. 17 as the particle size increases. The larger the terraces grow and the more well-ordered the adsorbed CO islands are, the more pronounced the intensity transfer in the IR spectra becomes. After all the intensity transfer is a collective phenomenon depending on the size of the active domain [133-135]. It is therefore, very dangerous to try to infer from the analysis of IR spectra information on the amount of adsorbate molecules present, or, for example, use IR to titrate the abundance of differently oriented facets in dispersed catalysts.

7. MAGNETIC PROPERTIES

In addition to investigations on electronic properties it is interesting to develop tools which allow us to study magnetic properties. Bases upon the experience we have developed with using electronic spin resonance (ESR) on radicals adsorbed on single crystal surfaces [136-138] we have started measurements of the ferromagnetic resonance (FMR) [139, 140]. To this end we prepare either a bulk single crystal oxide surface or an epitaxial thin oxide film under ultrahigh vacuum conditions and grow the metal aggregates on it. Such a sample is brought into a microwave cavity and the FMR is recorded. The sample, which is attached to a manipulator may be oriented with respect to the external field, and therefore the orientation of the direction of the magnetization is accessible.

Figure 20 shows such a measurement for Co particles on Al_2O_3(0001), deposited at room temperature. An uniaxial orientation is found with a single minimum at orientation of the field parallel to the surface plane. This means that the magnetization is also oriented in this way [140]. A very similar behaviour is found for iron as plotted in figure 20b. The smaller asymmetry is a property of the specific metal. While upon heating the behaviour does not change for CO, it becomes more complex for iron (see Fig. 21) [141]. This is indicative for the survival of uniaxial magnetism in the hexagonal cobalt and its breakdown for the body centered cubic iron. Fe(bcc) has three easy axes of magnetization and the formation of more crystalline aggregates is likely to be the reason for the observation.

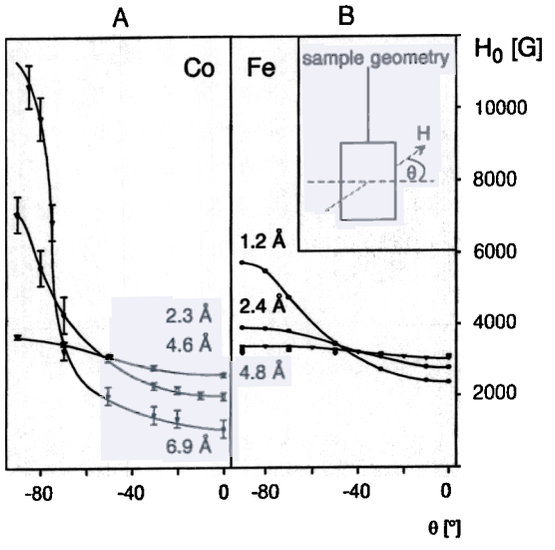

Figure 20. Angular dependence of the resonance field for various amounts of Co and Fe deposited at room temperature on an $Al_2O_3(0001)$-single crystal surface. θ denotes the angle between the crystal surface and the static magnetic field. The deposited amounts are given in terms of the effective layer thickness.

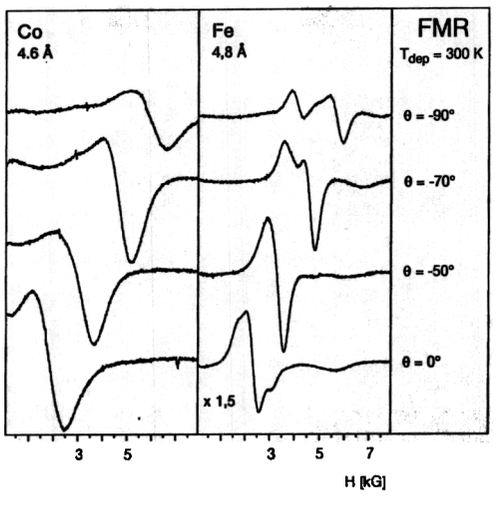

Figure 21. Comparison of the angular dependent FMR-spectra of Co and Fe on $Al_2O_3(0001)$ after heating the deposits prepared at 300 K to 870 K. The spectra were recorded at 300 K. θ denotes the angle between the static magnetic field and the crystal surface. The deposited amounts are given in terms of the effective layer thickness.

Since atomic resolution is very hard to achieve on the small aggregate at present, these experimental observations in the ferromagnetic resonance are very useful.

FMR can also be used to follow adsorption of the aggregates. We find that chemisorption of CO quenches the surface magnetism of the small particles. Oxidation of the small particles leads to the formation of an oxide skin on a ferromagnetic kernel. Since the oxide signal occurs at very different fields only the FMR of the kernel has been recorded. Such measurements may be used to follow the formation of oxide aggregates deposited on oxide supports which would have interesting catalytic properties.

8. PHOTOCHEMISTRY ON METAL AGGREGATES

Small deposited aggregates lend themselves to photochemical studies, in which the influences of the aggregate sizes on the photochemistry on the surface of the particles is explored. In particular, the photodesorption cross sections of small molecules such as NO and CO from Pd aggregates have been studied. In this case we heavily drew upon the experience described above. Another interesting molecule to study is methane.

Methane will become an increasingly important raw material in the next decades when more and more petrol resources will be exhausted [142]. The primary step of methane conversion into larger hydrocarbons is the cleavage of the CH-bond. However, one of the major difficulties in the use of methane is the rather elevated dissociation energy for cleaving the CH-bond of 113 kcal/mol in the gas phase [49]. Very often this is the rate limiting step for most technical relevant methane reactions for which high temperatures (>1000 K) and high pressures are actually necessary. The conditions can be marginally improved when using transition metals or transition metal oxids as catalysts.

For a photochemical cleavage of the CH bond in methane the conditions are not much better than for the thermal cleavage as the first optical allowed transition into a Rydberg state of methane leading to a bond breaking is situated in the VUV (i.e. implying the use of Lyman α-line of hydrogen at 121.6 nm). Recently, however, it has been discovered that photodissociation of methane is possible on Pt(111) and Pd(111) single crystal surfaces with laser light of 193 nm (6.4 eV) [143, 144].

For a technical application it is interesting to use noble metals with a favourable number of surface atoms with respect to bulk atoms to minimise the amount of metal necessary. A rather high percentage of surface atoms can be found in clusters containing less than 1000 atoms. Such clusters can be stabilised by fixation onto a support as has been realised for example for car exhaust catalysts. However, when reducing the cluster size, changes in the geometrical and electronic structure can occur changing the properties of the clusters compared to single crystals. Furthermore the properties of the clusters can be influenced by the interaction with the embedding medium (see above).

In order to systematically study the influence of cluster size and morphology on the photochemistry of methane we worked with our model systems described in previous chapters.

The data presented will focus on average cluster sizes between 450 - <1000 atoms per island.

Deuterated methane was photodissociated with a broad band excimer laser (Lambda Physik EMG 200) run at 6.4 eV with normal incidence on the surface. This excitation energy is below the band gap of the Al_2O_3 so that the major excitation occurs within the Pd-particles. The laser fluence was typically 2.5 mJ/cm^2 per pulse in most of the experiments with a pulse length of 15 ns and a repetition rate of 4 Hz.

As the surface area grows with increasing Pd-deposition a temperature programmed desorption (TPD) spectrum of a saturation coverage of deuterated methane was recorded as a measure of the total surface area available for methane adsorption prior to each photochemistry experiment. For a bare alumina surface no methane desorption peak was observed. The maximal temperature for the TPD spectra did not exceed 300 K, the growth temperature of the Pd-aggregates to avoid changes of the aggregate morphology. No fragmentation from simple deposition was observed. The maximum of the main desorption peak of undissociated methane shifts continuously towards lower temperature with decreasing cluster size. The TPD spectra of the smallest aggregates used in our experiments were shifted by 10 K as compared to the largest aggregates indicating a decrease of molecule surface interaction with decreasing cluster size. The peak area of the feature of m/e=20 was further used as reference for the total changes in methane concentration during the following photochemistry measurements including desorption and dissociation.

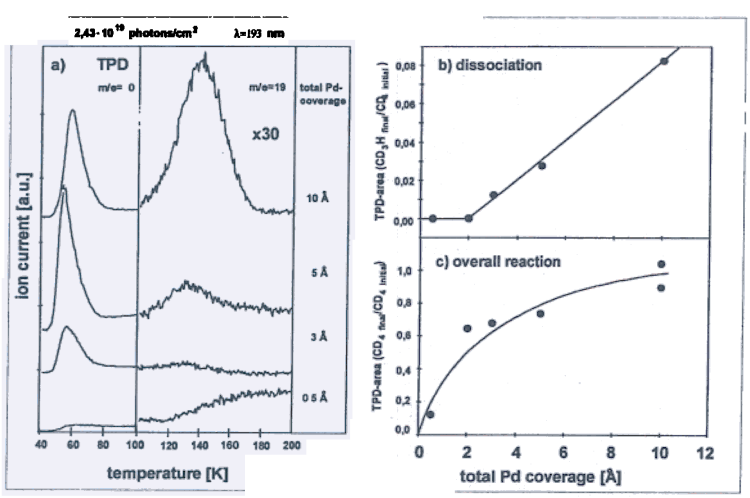

Figure 22: a) number of TPD spectra after exposure to 2.43·10^{19} photons/cm^2 of 6.4 eV as a function of Pd coverage; left column: m/e=20 (undissociated deuterated methane) right column: m/e=19 (recombinative desorption of deuterated methyl plus hydrogen)
b) surface area of the TPD spectra from the recombinative desorption of CD_3+H normalised to the initial coverage obtained from integrating the TPD spectra of the m/e=20 feature before laser irradiation as a function of Pd-coverage
c) integrated TPD area of the undissociated CD_4 normalised to the initial coverage as a function of Pd-coverage

Starting with a defined coverage of deuterated methane the system was exposed to a fixed number of photons impinging on the surface. The photochemistry presented here will be restricted to saturation coverages of methane. Fig.22a shows a number of TPD spectra after exposure to $1.5 \cdot 10^{19}$ photons/cm^2 as a function of Pd coverage. The left column corresponds to m/e=20 and is due to undissociated deuterated methane. The maximum of the TPD spectra turned out to be very sensitive to the coverage, the average cluster size and coadsorbates like atomic hydrogen from photodissociation which explains the different shifts of the main feature in those TPD spectra. The right column corresponds to recombinative desorption of CD_3+H (m/e=19). The hydrogen on the surface results from residual gas within the chamber and is due to the high sorbtivity of palladium with respect to hydrogen adsorption. As it turned out the background free TPD spectra of CD_3H were valuable for the photodissociation analysis particularly in case only small photodissociation rates were observed as the CD_4 TPD spectra were obscured by a small background from methane desorption from surfaces other than the crystal area. No other reaction products have been observed except for the mentioned recombinative desorption of CD_3+H/D.

Fig. 22b shows a plot of the normalised peak area of the TPD spectrum from the recombinative desorption of CD_3+H after exposure to $1.5 \cdot 10^{19}$ photons/cm^2 as a function of Pd-coverage. Normalisation is done by dividing the original peak area of the recombinative desorption by the peak area of the TPD spectrum from the initial coverage prior to photodissociation obtained from integrating the TPD spectrum of the m/e=20 feature. The graph clearly shows that photodissociation is only observed when the cluster size exceeds a certain threshold (average diameter per cluster: approximately 2.7 Å). For larger aggregates the photodissociation cross section increases with increasing cluster size. The probability for photodesorption behaves inversely, i.e. increases with decreasing cluster size. This is evident from Fig. 22c showing the integrated TPD area of the undissociated CD_4 normalised to the initial coverage as a function of Pd-coverage.

In single crystal experiments self quenching of photodissociation has been observed, i.e. after reaching a certain product concentration on the surface no further photodissociation could be observed [143, 144]. For example, when starting with a saturation coverage ca. 20% of the initial coverage remained unreacted on Pd(111) [144]. Similar observations have been obtained for the photodissociation of methane on Pt(111). For this system infrared experiments indicated that this is due to a reduced interaction of methane with the surface [145]. This self quenching is also observed for photochemistry on the clusters. However, it occurs at much lower concentrations. For the largest aggregates in our experiments for which the overall photoreaction cross section approaches the value of the single crystal surface ca. 85% of the initial coverage remained unreacted. This indicates that the overall electronic structure of the finite sized aggregates is easily perturbed by coadsorbates like CD_3 Though the main quenching effect could be attributed to adsorption of in single crystal experiments while atomic hydrogen did not show a measurable influence this still needs checking for the aggregates.

Single crystal experiments have shown that the initial excitation step is likely to occur within the adsorbate. Two models are actually discussed in the literature to explain the laser induced dissociation of methane on Pt(111) and Pd(111) [146-148].

The first model, a more chemical oriented model [146], is supported by ab initio cluster calculations for Pt (clusters from 1-10 atoms) [147]. It discusses a mixing of the unoccupied antibonding Rydberg state of methane (gas phase value: 8.5 eV) with unoccupied metal states to account for a broadening and a shift of the first electronically excited state so that the photodissociation at 6.4 eV becomes possible. The excitation energy of this state leading to dissociation to $CH_3 + H$ is strongly depending on the cluster size as the electron redistribution over the surrounding metal plays an important role to stabilise this charge transfer state [147]. Within this model a decrease of the cluster size causes a reduction of the delocalisation resulting in a shift of the excitation energy towards higher energies.

The second model argues that a reduction of the ionisation potential of methane due to the interaction with the metal accounts for the possibility to dissociate methane at 6.4 eV [148]. Starting from the vacuum level of Pd the Fermi level of the metal is situated 5.6 eV below the vacuum level according to workfunction measurements [149]. With reference to the vacuum level the HOMO (highest occupied molecular orbital) state of methane is 12.6 eV below the vacuum level considering the pure gas pase value [149]. A further attractive force due to the image charge resulting from the ionic excited state further stabilises this level by a shift towards the vacuum level [148]. Slab LDA calculations on CH_4/Pd(111) revealed that the equilibrium height between the Pd plane to the C nucleus of 3 Å above the surface [148] allows to use the image charge model of Jennison et al. [150] from which an estimate of 1.9 eV can be made for the attractive force. Assuming a low electron tunneling barrier between adsorbate and substrate one obtains an approximate minimum excitation energy of 5.1 eV to produce the dissociative state of cationic methane. Indeed no photodissociation could be observed on single crystals at excitation energies of 5.0 eV [143, 144]. The image potential will be strongly depending on the electronic structure and thus on the cluster size which explains a decrease in photodissociation probability. Furthermore, as the image-potential changes scale with $1/r$ (r being the equilibrium height of CH_4 above Pd), the dissociation efficiency might be strongly influenced by the cluster size which governs the actual interaction between methane and the substrate. This is supported by the observation that the peak maximum of TPD spectra of the undissociated methane shift towards lower temperatures with decreasing cluster size indicative for a diminishing interaction between the molecules and the surface thus increasing molecule-surface distance.

From chemical intuition one expects an increased lifetime of the excited state concomitant with the quantisation of the electronic states when reducing the cluster size which would increase the photodissociation probability. However, this effect appears to be less important than the influence of charge delocalisation within the cluster on the photodissociation threshold.

To summarise: Photodissociation and photodesorption of methane on Pd-aggregates of various sizes on a thin epitaxial Al_2O_3 support show very pronounced size effects. The observations can be understood assuming a strong reduction of charge delocalisation relevant for the photodissociation process when reducing the cluster size. These results are very promising with respect to giving a better insight into photoreactions on nanosized aggregates under such very defined conditions.

ACKNOWLEDGEMENTS

We thank the Deutsche Forschungsgemeinschaft, Bundesministerium für Bildung und Forschung, and Fonds der Chemischen Industrie for support. K. Watanabe and Y. Matsumoto took part in the studies of photochemistry on deposited aggregates.

REFERENCES

[1] Henrich, V.E., Cox, P.A.: The Surface Science of Metal Oxides, Cambridge University Press, Cambridge (1994).
[2] Freund, H.-J., Kuhlenbeck, H., Staemmler, V.: Rep. Progr. Phys. 59 (1996) 283.
[3] Renaud, G.: Surf. Sci. Rep. 32 (1998) 1.
[4] Campbell, C.T.: Surf. Sci. Rep. 27 (1997) 1.
Campbell, C.T.: Curr. Opin. Sol. State Mat. Sci. (1998) in press.
[5] Xu, C., Goodman, D.W., in Handbook of Heterogenous Catalysis, (Eds.: G. Ertl, H. Knözinger, J. Weitkamp) VCH, Weinheim (1997), Chapter 4.6.
[6] Freund, H.-J.: Angew. Chem. Int. Ed. 36 (1997) 452.
Bäumer, M., Libuda, J., Freund, H.-J., NATO ASI Series E, Kluwer Acad. Press, Vol 331 (1997), pages 61-104.
[7] Henry, C.: Surf. Sci. Rep. 31 (1998) 231.
[8] Nygren, M.A., Pettersson, L.G.M.: J. Chem. Phys. 105 (1996) 9339.
[9] Menges, M., Baumeister, B., Al-Shamery, K., Freund, H.-J., Fischer, C., Andresen, P.: J. Chem. Phys. 101 (1994) 3318.
[10] Klüner, T., Freund, H.-J., Staemmler, V., Kosloff, R.: Phys. Rev. Lett. 80 (1998) 5208 .
[11] Henzler, M., Göpel, W.: Oberflächenphysik des Festkörpers, Teubner, Stuttgart (1991).
[12] Neyman, K.M., Pacchioni, G., Kösch, N., in Recent Developments and Applications of Modern Density Functional Theory and Computational Chemistry, Vol 4, page 569 (1996).
[13] Pöhlchen, M., Staemmler, V.: J. Chem. Phys. 97 (1992) 2583.
[14] for CO on MgO powder samples see: Furuyama, S., Fujii, H., Kawamura, M., Morimoto, T.: J. Phys. Chem. 82 (1978) 1028
[15] Wichtendahl, R., Rodriguez-Rodrigo, M., Härtel, U., Kuhlenbeck, H., Freund, H.-J.: Surf. Sci., submitted.
[16] a) Vesecky, S.M., Xu, X., Goodman, D.W.: J. Vac. Sci. Technol. A 12 (1994) 2114.
b) He, J.W., Estrada, C.A., Corneille, J.S., Wu, M.C., Goodman, D.W.: Surf. Sci. 261 (1992) 164.
[17] Wichtendahl, R.: to be published.
[18] Cappus, D., Klinkmann, J., Kuhlenbeck, H., Freund, H.-J.: Surf. Sci. Lett. 325 (1995) L 421.
[19] Kuhlenbeck, H., Odörfer, G., Jäger, R., Illing, G., Menges, M., Mull, T., Freund, H.-J., Pöhlchen, M., Staemmler, V., Witzel, S., Scharfschwerdt, C., Wennemann, K., Liedtke, T., Neumann, M.: Phys. Rev. B 43 (1991) 1969

[20] Schönnenbeck, M., Cappus, D., Klinkmann, J., Freund, H.-J., Pettersson, L.G.M., Bagus, P.S., Surf. Sci 347 (1996) 337.
[21] Staemmler, V., in Adsorption on Ordered Surfaces of Ionic Solids and Thin Films, (Eds: H.-J. Freund, E. Umbach), Springer Series in Surface Science, Vol. 33, page 169, Springer Verlag Heidelberg (1993).
[22] Pacchioni, G., Cogliandro, G., Bagus, P.S.: Surf. Sci. 255 (1991) 344.
[23] Lindsay, R., Baumgärtel, P., Terbory, R., Schaff, O., Bradshaw, A.M., Woodruff, D.P.: Phys. Rev. Lett., submitted
[24] Dillmann, B., Rohr, F., Seiferth, O., Klivenyi, G., Bender, M., Homann, K., Yakovkin, I.N., Ehrlich, D., Bäumer, M., Kuhlenbeck, H., Freund, H.-J.: Farad. Disc. 105 (1996) 295
[25] Seiferth, O., Wolter, K., Dillmann, B., Klivenyi, G., Freund, H.-J., Scarano, D., Zecchina, A.: Surf. Sci., submitted
[26] Xu, C., Dillmann, B., Kuhlenbeck, H., Freund, H.-J.: Phys. Rev. Lett. 67 (1995) 3551.
[27] Bender, M., Ehrlich, D., Yakovkin, I.N., Rohr, F., Bäumer, M., Kuhlenbeck, H., Freund, H.-J.: J. Phys.: Cond. Mat. 7 (1995) 5289
[28] Hemmerich, I., Rohr, F., Seiferth, O., Dillmann, B., Freund, H.-J.: Z. Phys. Chem. 202 (1997) 31
[29] Rohr, F., Bäumer, M., Freund, H.-J., Mejias, J.A., Staemmler, V., Müller, S., Hammer, L., Heinz, K: Surf. Sci. 372 (1997) L291, Erratum Surf. Sci. 389 (1997) 391.
[30] Kuhlenbeck, H.: Appl. Phys. A 59 (1995) 469.
[31] Mejias, J.A., Staemmler, V., Freund, H.-J.: in preparation.
[32] Zimmermann, F.M., Ho, W.: Surf. Sci. Rep. 22 (1995) 127.
[33] Mull, T., Baumeister, B., Menges, M., Freund, H.-J., Weide, D., Fischer, C., Andresen, P.: J. Chem. Phys. 96 (1992) 7108.
[34] Freund. H.-J.: "Clean and Modified Oxide Surfaces: Structure and Dynamics of Adsorbed Molecules", Metal-Ligand Interactions: Structure and Reactivity (Eds.: N. Russo, D.R. Salahub), NATO ASI Series C Vol 474, Kluwer Acad. Press (1996), p 232
[35] Menzel, D., Gomer, R.: J. Chem. Phys. 41 (1964) 3311
Redhead, P.A.: Can. J. Phys. 42 (1964) 886.
[36] Antoniewicz, P.R.: Phys. Rev. B 21 (1980) 3811.
[37] Hasselbrink, E.: Chem. Phys. Lett. 170 (1990) 329.
[38] Gortel, Z.W., Wierzbicki, A.: Phys. Rev. B 43 (1991) 7487.
[39] Brenig, W.: Z. Physik B 23 (1976) 361.
[40] Saalfrank, P.: Chem. Phys. 193 (1995) 119.
[41] Burns, A.R., Stechel, E.B., Jennison, D.R.: Phys. Rev. Lett. 58 (1987) 250.
[42] Thiel, S., Klüner, T., Freund, H.-J.: Chem. Phys., in press.
[43] Sauer, J., Ugliengo, P., Garrone, E., Saunders, V.R.: Chem. Rev. 94 (1994) 2095.
[44] Gross, A., Scheffler, M.: Phys. Rev. B 57 (1998) 2493.
[45] Guo, H., Chen, F.: Faraday Discussions 108 (1997) 309.

[46] Klüner, T., Freitag, J., Freund, H.-J., Staemmler, V.: J. Chem. Phys. 104 (1996) 10030.
[47] Klüner, T., Thiel, S., Freund, H.-J., Staemmler, V., Kosloff, R.: to be published.
[48] Klüner, T., Thiel, S., Freund, H.-J., Staemmler, V.: Proceedings of the SPIE'S/LASER '98 conference, 3272 (1998) 177.
[49] Huber, K.P., Herzberg, G.: Constants of diatomic molecules, Van Nostrand Reinhold, New York (1979).
[50] Baumeister, B., Freund, H.-J.: J. Phys. Chem. 98 (1994) 11962.
[51] Kosloff, R.: J. Phys. Chem. 92 (1988) 2087.
[52] Gadzuk, J.W.: Surf. Sci. 342 (1995) 345.
[53] Klüner, T., Freitag, J., Freund, H.-J., Staemmler, V.: J. Mol. Catal. A, 119 (1997) 155.
[54] Klüner, T., Thiel, S., Freund, H.-J., Kosloff, R.: Isr. J. Chem., submitted.
[55] Klüner, T., Thiel, S., Freund, H.-J., Staemmler, V.: Chem. Phys. Lett., in press.
[56] Lambert, R.M., Pacchioni, G.(Eds.): Chemisorption and Reactivity on Supported Clusters and Thin Films, NATO ASI Series, Series E, 331, Kluwer, Dordrecht, 1997
[57] Wu, M.C., Estrada, C.A., Corneille, J.S., Goodman, D.W.: J. Chem. Phys. 6 (1992) 3892.
[58] Wu, M.C., Truong, C.M., Goodman, D.W.: J. Phys. Chem. 9 (1993) 4182.
[59] He, J.W., Corneille, J.S., Estrada, C.A., Wu, M.C., Goodman, J.D.W.: Vac. Sci. Technol. A 10 (1992) 2248.
[60] Heidberg, J., Meine, D.: Ber. Bunsenges. Phys. Chem. 97 (1993) 211.
[61] Henzler, M., Stock, A., Böl, M.: In: Adsorption On Ordered Surfaces Of Ionic Solids And Thin Films, (Eds.: Freund, H.-J., Umbach, E.), Springer Series in Surface Sciences 33, Springer Verlag, Heidelberg, 1993.
[62] Schwennicke, C., Schimmelpfennig, J., Pfnür, H.: Surf. Sci. 293 (1993) 57.
[63] Truong, C.M., Wu, M.C., Goodman, D.W.: J. Am. Soc. 115 (1993) 3647.
[64] Zecchina, A., Scarano, D., Bordiga, S., Ricchiardi, G., Spoto, G., Geobaldo, F.: Catal. Today 27 (1996) 403.
[65] Schröder, K.M., Schäfer, F., Wollschläger, J., Henzler, M.: Surf. Sci. Submitted.
[66] Jaeger, R.M., Kuhlenbeck, H., Freund, H.-J., Wuttig, M., Hoffmann, W., Franchy, R., Ibach, H.: Surf. Sci. 259 (1991) 235.
[67] Wuttig, M., Hoffmann, W., Jaeger, R.M., Kuhlenbeck, H., Freund, H.-J.: Mat. Res. Soc. Symp. Proc. 221 (1991) 143.
[68] Jaeger, R.M., Homann, K., Kuhlenbeck, H., Freund, H.-J.: Chem. Phys. Lett. 203 (1993) 41.
[69] Jaeger, R.M., Libuda, J., Bäumer, M., Homann, K., Kuhlenbeck, H., Freund, H.- J.: J. Electron Spectrosc. Relat. Phenom. 64/65 (1993) 217.
[70] Libuda, J., Bäumer, M., Freund, H.-J.: J. Vac. Sci. Technol. A 12 (1994) 2259.
[71] Libuda, J., Winkelmann, F., Bäumer, M., Freund, H.-J., Bertrams, Th., Neddermeyer, H., Müller, K.: Surf. Sci. 318 (1994) 61.
[72] Chen, P.J., Goodman, D.W.: Surf. Sci. Lett. 318 (1994) L767.

[73] Wu, Y., Tao, H.-S., Garfunkel, E., Madey, T.E., Shinn, N.D.: Surf. Sci. 336 (1995) 123.
[74] Wu, Y., Garfunkel, E., Madey, T.E., In Preparation.
[75] Stempel, S.: Phd Thesis, Freie Universität Berlin, In Preparation.
[76] Libuda, J.: Phd Thesis, Ruhr-Universität Bochum 1996.
[77] Libuda, J., Sandell, A., Bäumer, M., Freund, H.-J.: Chem. Phys. Lett. 240 (1995) 429.
[78] Libuda, J., Frank, M., Sandell, A., Andersson, S., Brühwiler, P.A., Bäumer, M., Mårtensson, N., Freund, H.-J., In: Elementary Processes And Excitations And Reactions On Solid Surfaces, Springer Series In Solid State Sciences, 121, 1996, P. 210-216.
[79] Freund, H.-J., Dillmann, B., Ehrlich, D., Hassel, M., Jaeger, R.M., Kuhlenbeck, H., Ventrice, C.A., Winkelmann, F., Wohlrab, S., Xu, C., Bertrams, Th., Brodde, A., Neddermeyer, H.: J. Mol. Catal. 82 (1993) 143.
[80] Winkelmann, F., Wohlrab, S., Libuda, J., Bäumer, M., Cappus, D., Menges, M., Al-Shamery, K., Kuhlenbeck, H., Freund, H.-J.: Surf. Sci. 307-309 (1994) 148.
[81] Wohlrab, S., Winkelmann, F., Libuda, J., Bäumer, M., Kuhlenbeck, H., Freund, H.-J. In: Surface Science Principles And Applications, Eds. Macdonald, R.J., Taglauer, E.C., Wandelt, K., Springer, Berlin 1996, P. 193-202.
[82] Bertrams, Th., Winkelmann, F., Uttich, Th., Freund, H.-J., Neddermeyer, H.: Surf. Sci. 331-333 (1995) 1515.
[83] Bäumer, M., Libuda, J., Sandell, A., Winkelmann, F., Freund, H.-J., Graw, G., Bertrams, Th., Neddermeyer. H.: Ber. Bunsenges. Phys. Chem. 99 (1995) 1381.
[84] Sandell, A., Libuda, J., Brühwiler, P., Andersson, S., Maxwell, A.J., Bäumer, M., Mårtensson, N., Freund, H.-J.: J. Electron Spectrosc. Relat. Phenom. 76 (1995) 301.
[85] Sandell, A., Libuda, J., Bäumer, M., Freund, H.-J.: Surf. Sci. 346 (1996) 108.
[86] Sandell, A., Libuda, J., Brühwiler, P.A., Andersson, S., Bäumer, M., Maxwell, A.J., Mårtensson, N., Freund, H.-J.: Phys. Rev. B 55 (1997) 7233.
[87] Sandell, A., Libuda, J., Brühwiler, P.A., Andersson, S., Bäumer, M., Maxwell, A.J., Mårtensson, N., Freund, H.-J.: J. Vac. Sci. Technol. A 14 (1998) 1546.
[88] Gaylord, R.H.: Phd Thesis, University Of Pennsylvania 1987.
[89] Mundenar, J.M.: Phd Thesis, University Of Pennsylvania 1988.
[90] Almy, D.B., Foyt, D.C., White, J.M.: J. Electron Spectrosc. Relat. Phenom. 11 (1977) 129.
[91] Paul, J., Hoffmann, F.M.: J. Phys. Chem. 21 (1986) 5321.
[92] Coustet, V., Jupille, J.: Surf. Sci. 309 (1994) 309; Surf. Interface Anal. 22 (1994) 280.
[93] Frederick, B.G., Apai, G., Rhodin, T.N.: Surf. Sci. 244 (1991) 67.
[94] Schildbach, M.A., Hamza, A.V.: Surf. Sci. 282 (1993) 306.
[95] Mcdonald, J.E., Eberhart, J.G.: Trans. Met. Soc. Aime 233 (1965) 512.
[96] Chatain, D., Rivollet, I., Eustathopoulos, N.: J. Chim. Phys. 83 (1986) 561, Ibid 84 (1987) 201.
[97] Bauer, E.: Zeitschrift Für Kristallographie 110 (1958) 372.

[98] Libuda, J., Frank, M., Sandell, A., Andersson, S., Brühwiler, P.A., Bäumer, M., Mårtensson, N., Freund, H.-J.: Surf. Sci. 384 (1997) 106.
[99] Klimenkov, M., Nepijko, S.A., Kuhlenbeck, H., Bäumer, M., Schlögl, R., Freund, H.-J.: Surf. Sci. 391 (1997) 27.
[100] Nepijko, S.A., Klimenkov, M., Kuhlenbeck, H., Zemlyanov, D., Herein, D., Schlögl, R., Freund, H.-J.: Surf. Sci., In Press.
[101] Nepijko, S.A., Klimenkov, M, Adelt, M., Kuhlenbeck, H., Schlögl, R., Freund, H.-J.: Langmuir, Submitted.
[102] Hansen, K.H., Stempel, S., Bäumer, M., Stensgaard, I., Besenbacher, F., Freund, H.-J., Unpublished.
[103] Frank, M., Andersson, S., Libuda, J., Stempel, S., Sandell, A., Brena, B., Giertz, A., Brühwiler, P.A., Bäumer, M., Mårtensson, N., Freund, H.-J.: Chem. Phys. Lett. 279 (1997) 92.
[104] Frederick, B.G., Apai, G., Rhodin, T.N.: J. Am. Chem. Soc. 109 (1987) 4797.
[105] Mason, M.G.: Phys. Rev. B 27 (1983) 748.
[106] Wertheim, G.K.: Z. Phys. B 66 (1987) 53.
[107] Wertheim, G.K.: Z. Phys. D 12 (1989) 319.
[108] Wertheim, G.K., Dicenzo, S.B., Buchanan, D.N.E.: Phys. Rev. B 33 (1986) 5384.
[109] Marks, F.A., Lindau, I., Browning, R.: J. Vac. Sci. Technol. A 8 (1990) 3437.
[110] Schönhammer, K., Gunnarsson, O.: Solid State Commun. 23 (1977) 691.
[111] Schönhammer, K.S., Gunnarsson, O.: Z. Phys. B 30 (1978) 297.
[112] Dicenzo, S.B., Wertheim, G.K.: Comm. Solid State Phys. 11 (1985) 203.
[113] Ogawa, S., Ichikawa, S.: Phys. Rev. B 51 (1995) 17231.
[114] Sarapatka, T.J.: J. Phys. Chem. 97 (1993) 11274.
[115] Sarapatka, T.J.: Chem. Phys. Lett. 212 (1993) 37.
[116] Freund, H.-J., Neumann, M.: Appl. Phys. A 47 (1988) 3.
[117] Freund, H.-J.: Handbook Of Heterogeneous Catalysis (Eds.: Ertl, G., Knözinger, H., Weitkamp, J.) Part A Chapter 5.1, Section 5.1.1 Principles Of Chemisorption, 1997.
[118] King, D.A., Woodruff, D.P.: The Chemical Physics Of Solid Surfaces And Heterogeneous Catalysis, 3, Chemisorption Systems, Part A, Elsevier 1990.
[119] Mårtensson, N., Nilsson, A. in Applications Of Synchrotron Radiation, Springer Series In Surface Sciences, Vol. 35, (Ed.:Eberhardt, W.), Springer, Berlin 1995.
[120] Andersen, J.N., Quarford, M., Nyholm, R., Sorensen, S.L., Wigren, C.: Phys. Rev. Lett. 67 (1991) 2822.
[121] Andersen, J.N., Hennig, D., Lundgren, E., Methfessel, M., Nyholm, R., Scheffler, M.: Phys. Rev. B 50 (1994) 7525.
[122] Björneholm, O., Nilsson, A., Tillborg, H., Bennich, P., Sandell, A., Hernnäs, B., Puglia, C., Mårtensson, N.: Surf. Sci. 315 (1994) L983.
[123] Adelt, M., Nepijko, S., Drachsel, W., Freund, H.-J.: Chem. Phys. Lett. 291 (1998) 437.
[124] Wolter, K., Seiferth, O., Kuhlenbeck, H., Bäumer, M., Freund, H.-J.: Surf. Sci. 399 (1998) 190.
[125] Badri, A., Binet, C., Lavalley, J.-C.: J. Chem. Soc. Faraday Trans. 92 (1992) 1603.

[126] Rainer, D.R., Wu, M.-C., Mahon, D.I., Goodman, D.W.: J. Vac. Sci. Technol. A 14 (1996) 1184.

[127] Evans, J., Hayden, B.E., Lu, G.: Surf. Sci. 360 (1996) 61.
[128] Tüshaus, M.: Phd Thesis, Berlin 1990.
[129] Tüshaus, M., Berndt, W., Conrad, H., Bradshaw, A.M., Persson, B.: Appl. Phys. A 51 (1990) 91.
[130] Kuhn, W.K., Szanyi, J., Goodman, D.W.: Surf. Sci. Lett. 274 (1992) L611.
[131] Fernandez, V., Gießel, T., Schaff, O., Schindler, K.-M., Theobald, A., Hirschmugl, C.J., Bao, S., Bradshaw, A.M., Baddeley, C., Lee, A.F., Lambert, R.M., Woodruff, D.P., Fritzsche, V.: Z. Phys. Chem. 198 (1997) 73.
[132] Van Hardeveld, R., Hartog, F.: Surf. Sci. 15 (1969) 189.
[133] Hollins, P., Pritchard, J.: Prog. Surf. Sci. 19 (1985) 275.
[134] Hollins, P.: Surf. Sci. Rep. 16 (1992) 51.
[135] Persson, B.N.J., Ryberg, R.: Phys. Rev. B 24 (1981) 6954.
[136] Schlienz, H., Beckendorf, M., Katter, U.J., Risse, T., Freund, H.-J.: Phys. Rev. Lett. 74 (1995) 761.
[137] Katter, U.J., Hill, Th., Risse, T., Schlienz, H., Beckendorf, M., Klüner, Th., Hamann, H., Freund, H.-J.: J. Phys. Chem. B 101 (1997) 552.
[138] Risse, T., Hill, Th., Schmidt, J., Abend, G., Hamann, H., Freund, H.-J.: J. Chem. Phys. 108 (1998) 9615.
[139] Hill, Th., Mozaffari-Afshar, M., Schmidt, J., Risse, T., Stempel, S., Heemeier, M., Freund, H.-J.: Chem. Phys. Lett. 292 (1998) 524.
[140] Hill, Th., Stempel, S., Risse, T., Bäumer, M., Freund, H.-J.: J. Magn. Mag. Mater., submitted.
[141] Hill, Th.: PhD Thesis, Ruhr-Universität Bochum, in preparation.
[142] Seshan, K., Lercher, J.A. in Carbon Dioxide Chemistry: Environmental Issues (Eds.: J. Paul and Claire-Marie Pradier), The Royal Society of Chemistry (1994)
[143] Gruzdkov, Y.A., Watanabe, K., Sawabe, K., Matsumoto, Y.: Chem. Phys. Lett. 227 (1994) 243
[144] Watanabe, K., Matsumoto, Y.: paper submitted
[145] Yoshinobu, J., Ogasawara, H., Kawai, M.: Phys. Rev. Lett. 75 (1995) 2176
[146] Matsumoto, Y., Gruzdkov, Y.A., Watanabe, K., Sawabe, K.: J. Chem. Phys. 105 (1996) 4775
[147] Akinaga, Y., Taketsugu, T., Hirao, K.: J. Chem. Phys. 107 (1997) 415
[148] Jennison, D.R.: private communication
[149] D. R. Lide (Ed.): Handbook of Chemistry and Physics, (CRC Press, Boca Raton,1997-1998)
[150] Jennison, D.R., Stechel, E.B., Burns, A.R., Li, Y.S.: Nuc. Instr. Meth. Phys. Res. B101 (1995) 22